analytical chemistry

Article

pubs.acs.org/ac

A Method of Cryoprotection for Protein Crystallography by Using a Microfluidic Chip and Its Application for in Situ X-ray Diffraction Measurements

Masatoshi Maeki,*[,†,‡,§] Ashtamurthy S. Pawate,[∥] Kenichi Yamashita,[†,§] Masahide Kawamoto,[⊥] Manabu Tokeshi,[‡] Paul J. A. Kenis,[∥] and Masaya Miyazaki*[,†,§]

[†]Department of Molecular and Material Sciences, Interdisciplinary Graduate School of Engineering Sciences, Kyushu University, 6-1 Kasuga-Koen, Kasuga, Fukuoka 816-8580, Japan

[‡]Division of Biotechnology and Macromolecular Chemistry, Faculty of Engineering, Hokkaido University, Kita 13 Nishi 8, Kita-ku, Sapporo 060-8628, Japan

[§]Advanced Manufacturing Research Institute, National Institute of Advanced Industrial Science and Technology, 807-1 Shuku, Tosu, Saga 841-0052, Japan

[∥]Department of Chemical and Biomolecular Engineering, University of Illinois at Urbana−Champaign, 600 South Mathews Avenue, Urbana, Illinois 61801, United States

[⊥]Kyushu Synchrotron Light Research Center, 8-7 Yayoigaoka, Tosu, Saga 841−0051, Japan

ABSTRACT: We demonstrate a seamless and contactless method from protein crystallization to X-ray analysis using a microfluidic chip with the aim of obtaining a complete crystallographic data set of a protein crystal under cryogenic conditions. Our microfluidics-based approach did not require direct manipulation of the protein crystal. Therefore, the microfluidic chip approach is suitable for novices of X-ray analysis of protein crystals. We also investigated the effect of stepwise cryoprotection on the quality of protein crystals. Protein crystals with cryoprotection via on-chip manipulation did not show deterioration of crystallographic quality of the protein crystal. The complete diffraction data set of a protein crystal, which is required for determining the 3D structure of the target protein, is obtainable by a simple manipulation.

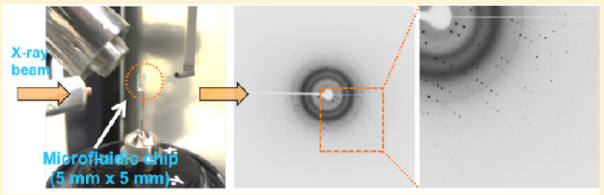

Protein crystallization coupled with 3D structure analysis is of significant research interest not only in the scientific world but also in industry, including drug discovery.[1−4] A variety of techniques for protein crystallization and X-ray analysis have been developed to elucidate the 3D structures of proteins.[5−10] Generally, protein structure determination is divided into three processes: preparation of the target protein, protein crystallization, and X-ray crystal structure analysis. The preparation process, which includes expression and purification, is the first step for protein crystallization, and preparation of a protein sample is often labor-intensive and time-consuming. The large-scale preparation of a target protein required for crystallization is also difficult, notably membrane protein expression is quite low. In the crystallization process, screening of protein crystallization conditions is carried out to generate suitable protein crystals. To prepare suitable protein crystals for X-ray crystal structure analysis, the screening of protein crystallization conditions is conducted several times. Protein crystals obtained by the screening of protein crystallization conditions are evaluated by X-ray analysis. In the X-ray crystal structure analysis, the protein crystal undergoes cryoprotection, a pretreatment prior to X-ray crystal structure analysis.[11,12] After cryoprotection, the treated protein crystal is mounted onto the X-ray diffractometer and cooled immediately by a cold nitrogen gas stream at 100 K. Protein crystallization and X-ray diffraction experiments are the main processes in structure determination by X-ray crystallography. In conventional methods, these processes are independent, so developing an integrated system or device is strongly desired.

Recently, microfluidic-technology-based platforms have been developed as a useful tool for protein crystallization and X-ray analysis.[13−18] Two types of crystallization platforms were reported: the droplet-based crystallization platform and the well-based crystallization platform. In both platforms, protein crystallization devices offer high-throughput screening of protein crystallization conditions, low amounts of sample consumption, and in situ X-ray diffraction experiments. This microfluidic-technology-based approach can conduct protein crystallization followed directly by in situ X-ray diffraction experiments. Clear X-ray diffraction patterns were obtained by using a microfluidic chip without any additional manipulation. Moreover, the development and application of a large synchrotron source facility has accelerated the structure determination of proteins. Here, high-flux synchrotron X-ray

Received: October 8, 2014
Accepted: April 3, 2015
Published: April 3, 2015

DOI: 10.1021/acs.analchem.5b00151
Anal. Chem. 2015, 87, 4194−4200

beamlines are employed for measuring protein microcrystals (~10 μm).[19,20] However, high-flux X-ray beams induce radiation damage to protein crystals because of the generation of oxygen radicals. To reduce radiation damage, X-ray diffraction experiments are usually carried out under a low-temperature gas flow at l00 K. The liquid inside or around the protein crystal must freeze into an amorphous, glassy state to avoid diffraction from ordered ice. Hence, cryoprotection is a significant process and an indispensable technique for obtaining a complete crystallographic data set from a sample.

Generally, protein crystallization and X-ray analysis experiments depend strongly on technique and experience, regardless of whether a conventional method or a microfluidics-based approach is used. Briefly, the protein crystal is soaked in the cryoprotection solution (cryoprotectant). The cryoprotectant contains the precipitant solution and a high concentration of glycerol, ethylene glycol, or sugar. Thus, the cryoprotected protein crystal has the potential to be damaged because of osmotic shock. Additionally, protein crystals are fragile because they contain water. The cryoprotection procedure requires highly skilled handling of the crystals. Therefore, the development of a contactless procedure for cryoprotection and X-ray analysis is desirable. Microfluidic devices enable a contactless approach and eliminate potential damage to samples, and on-chip X-ray diffraction experiments are suitable options.[21−24] However, on-chip cryoprotection and X-ray analysis of a protein crystal have not been well investigated. Therefore, cryoprotection remains a limitation for in situ X-ray diffraction studies using a microfluidic chip. In this paper, we demonstrate a seamless and contactless method from protein crystallization to X-ray analysis using a microfluidic chip with the aim of obtaining a complete crystallographic data set of a protein crystal under cryogenic conditions. We also investigate the effect of stepwise cryoprotection on the quality of the protein crystal.

EXPERIMENTAL SECTION

Preparation of Crystallization Solutions. Hen egg white lysozyme was purchased from Seikagaku Biobusiness Corporation (Tokyo, Japan). The lysozyme stock solution was prepared by dissolving an appropriate amount of lysozyme in 100 mM sodium acetate buffer (pH 4.5, Wako Pure Chemicals, Osaka, Japan) to obtain a concentration of 80 mg/mL. The concentration of lysozyme was determined by measuring the absorbance at 280 nm (Nano Drop 1000, Thermo Fisher Scientific, Wilmington, DE, USA) using an extinction coefficient of 2.65.[25] The precipitant solution was prepared by dissolving 1.4 M NaCl (Wako Pure Chemicals) in 100 mM sodium acetate buffer at pH 4.5. The cryoprotectant solution was prepared by dissolving 1.0 M NaCl and 40% glycerol (Wako Pure Chemicals) in 100 mM sodium acetate buffer at pH 4.5. All solutions were filtered through a 0.20 μm syringe filter (Minisart RC4 or RC25, Sartorius Stedim Biotech, Gottingen, Germany) prior to use in the protein crystallization experiments.

Fabrication of the Microfluidic Chip. The microfluidic chip was composed of a thin polydimethylsiloxane (SILPOT 184 W/C, Dow Corning Toray, Tokyo, Japan) fluid and a control layer sandwiched between a cyclic olefin copolymer (COC, TOPAS 6013, TOPAS Advanced Polymers, Florence, KY, USA). The COC thin film shows low gas permeability and high X-ray transmission properties. These properties are attractive features for fabrication and evaluation of a protein crystallization platform. For this reason, we used a PDMS−COC combined microfluidic chip for the protein crystallization platform. The microfluidic chip was fabricated using a standard soft lithographic procedure reported previously with minor modifications.[26,27] Briefly, SU-8 3050 was purchased from MicroChem (Westborough, MA, USA). SU-8 was poured onto silicon substrates and spin-coated to a thickness of 50 μm. After spin-coating, the fluid layer (FL) and control layer (CL) molds were made by standard photolithography. The master molds were treated with a vapor of trichloro (1*H*,1*H*,2*H*,2*H*-perfluorooctyl) silane (Sigma-Aldrich, St. Louis, MO, USA). The FL and CL of the PDMS thin layers were also obtained via spin-coating, and the thickness of these layers was 70 μm. The spin-coated silicon substrates were cured at 80 °C. The CL layer and COC thin film (50 μm) were treated with oxygen plasma for 90 s followed by bonding to each other to make the COC−CL assembly. The COC−CL assembly was cured at 80 °C for 5 min and cut out from the silicon substrate. The COC−CL assembly was aligned and placed on the FL substrate. The COC−CL−FL (COC−PDMS) assembly was heated for at least 4 h at 80 °C. Subsequently, the COC−PDMS assembly was cut out from the silicon substrate. Finally, the microfluidic chip was obtained by assembling the COC−PDMS layer and a COC thin film. Figure 1 shows a schematic illustration of the COC−PDMS microfluidic chip. There are 24 and 6 crystallization chambers for the standard microfluidic chip and the microfluidic chip for cryoprotection, respectively. The size of the crystallization chamber is 0.67 mm (width) × 0.75 mm (height) × 50 μm (depth). The thickness of the COC−PDMS microfluidic chip was 240 μm. The mechanism of the normally closed valve was reported previously.[16,28] The crystallization and cryoprotection solutions were mixed via normally closed valves, as shown in Figure 2.

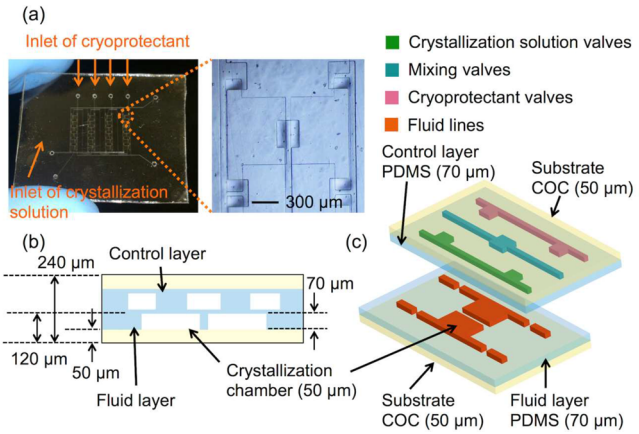

Figure 1. (a) Photographs of the standard COC−PDMS microfluidic chip and the crystallization chamber. There are 24 and 6 crystallization chambers for the standard microfluidic chip and the microfluidic chip for cryoprotection, respectively. The size of the crystallization chamber is 0.67 mm (width) × 0.75 mm (height) × 50 μm (depth). (b) Cross-sectional view of the microfluidic chip. The thickness of the COC−PDMS microfluidic chip is 240 μm. (c) 3D perspective view of the fluid and the control layer.

On-Chip Protein Crystallization and Cryoprotection Procedure. An equal volume of 80 mg/mL lysozyme solution and 1.4 M NaCl were premixed into a microtube. Thus, the final concentration of the crystallization solution was 40 mg/mL lysozyme and 0.7 M NaCl in 100 mM acetate buffer. Figure

DOI: 10.1021/acs.analchem.5b00151
Anal. Chem. 2015, 87, 4194−4200

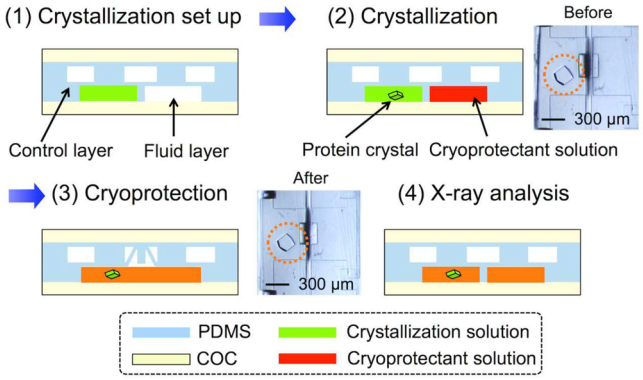

Figure 2. Schematic illustration of the protein crystallization and cryoprotection procedure via on-chip manipulation. (1) Premixed crystallization solution was introduced to the crystallization chamber (left) by a vacuum pump. (2) After protein crystallization (24−48 h), the cryoprotectant solution was also introduced to the cryoprotectant chamber (right). The photograph (top right) represents a lysozyme crystal within a crystallization chamber before cryoprotection. (3) Cryoprotectant solution and crystallization solution were mixed by counterdiffusion via the mixing valve. The mixing time per one manipulation was changed to 5, 10, and 30 min. The total mixing time was fixed at 30 min. The photograph (bottom left) represents a lysozyme crystal within a crystallization chamber after cryoprotection. (4) After cryoprotection, the crystallization chamber and cryoprotection chamber were separated by the normally closed valve.

2 shows a schematic illustration of the protein crystallization and cryoprotection procedure via on-chip manipulation.

The crystallization solution was pipetted onto the microfluidic chip and introduced to the crystallization chamber (left side) by a vacuum pump. These manipulations were monitored under the optical microscope (Eclipse TS100, Nikon, Tokyo, Japan). The microfluidic chip containing the crystallization solution was sealed by Crystal Clear Tape (Hampton Research, Aliso Viejo, CA, USA) and stored in an incubator at 20 °C. After lysozyme crystallization, cryoprotection of the lysozyme crystal was also carried out via on-chip manipulation. The cryoprotectant solution that contains 1.0 M NaCl, 40% glycerol, and 100 mM sodium acetate buffer (pH 4.5) was pipetted onto the microfluidic chip and introduced to the cryoprotectant chamber (right side). Then, the cryoprotectant solution and crystallization solution was mixed by counter-diffusion via the mixing valve. The final concentration of the cryoprotectant solution was 0.85 M NaCl, 20% glycerol, and 100 mM sodium acetate buffer.[29] To confirm the effect of stepwise cryoprotection, the mixing time per one manipulation was changed to 5, 10, and 30 min. The total mixing time was fixed at 30 min. For example, in the case of the 10 min mixing, this mixing manipulation was repeated three times for complete mixing with 5 min incubation between each manipulation. The microfluidic chip was sealed by Crystal Clear Tape and placed in an incubator at 20 °C until the X-ray diffraction experiment was conducted.

Diffraction Data Collection. We prepared lysozyme crystals using two sizes of microfluidic chip. Lysozyme crystals prepared by both microfluidic chips were analyzed by X-ray diffraction on a synchrotron source (BL 07 at the SAGA Light Source, Saga, Japan). The diffraction data set (90 images) was collected at a wavelength of 1.5 Å, with a 30 s exposure and 1° oscillation. Measurement temperature was 100 and 277 K for the cryogenic lysozyme crystal and the lysozyme crystal without cryoprotection, respectively. The mounted CryoLoop (HR4−615, Hampton Research, Aliso Viejo, CA, USA), which removed a loop part, was bonded to the CrystalCap Magnetic Ported (HR4−731, Hampton Research) by superglue. In the case of the cryocooling X-ray diffraction experiment, the microfluidic chip containing lysozyme crystals was cut to 5 × 5 mm^2. Then, the microfluidic chip was bonded onto the tip of a mounted CryoLoop by superglue. The lysozyme crystal subjected to cryoprotection was mounted onto a magnetic goniometer. The mounted microfluidic chip containing the lysozyme crystal was immediately cooled in a cold nitrogen gas stream at 100 K. Complete diffraction data sets were obtained using a CCD detector system (Saturn A200, Rigaku, Tokyo, Japan). The collected diffraction data was analyzed by XDS software and the CCP4 suite of programs.[30,31] The images of the diffraction pattern were also generated using the program iMosflm.

RESULTS AND DISCUSSION

Lysozyme crystals were obtained in all crystallization chambers after incubation at 20 °C. After lysozyme crystallization, cryoprotection of the lysozyme crystals was also carried out via on-chip manipulation (Figure 2). As shown in Figure 2, any cracks to the lysozyme crystal because of the cryoprotection process were not observed under the optical microscope measurement. This result indicates that the lysozyme crystal was not heavily damaged by cryoprotection. Then, we examined the effect of the size of the microfluidic chip on cryoprotection and optimized the size for obtaining a clear X-ray diffraction pattern under the cryogenic condition. Figure 3

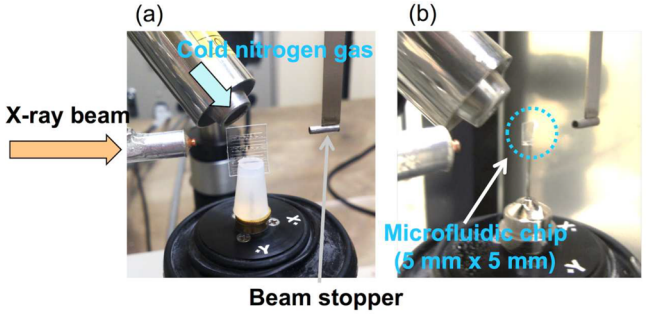

Figure 3. Comparison of the cooling situation of the microfluidic chip by cold nitrogen gas. (a) Photograph of the in situ X-ray diffraction experiment using a standard microfluidic chip at 277 K. (b) Photograph of a microfluidic chip that was cut to a size of 5 × 5 mm^2. This microfluidic chip was used for the X-ray diffraction experiment at 100 K.

shows photographs of the microfluidic chips used in this study. First, we used a standard COC−PDMS microfluidic chip, as reported previously.[23] The size of the standard microfluidic chip was almost 3 × 4 cm^2. After cryoprotection, the microfluidic chip was mounted onto a magnetic goniometer with a rubber stopper (Figure 3a). In the case of the standard microfluidic chip, frost was immediately observed on the opposite side of the microfluidic chip that was receiving a flow of cold nitrogen gas at 100 K. Moreover, the lysozyme crystal containing the microfluidic chip turned white. The change in the color of the lysozyme crystal indicates the generation of an ice crystal. As a result, an ice ring that was diffracted from water molecules was observed at ∼3.0 Å.[32,33] The ice ring presumably gives rise to the high background. The standard microfluidic

DOI: 10.1021/acs.analchem.5b00151
Anal. Chem. 2015, 87, 4194−4200

chip was not placed completely in the nitrogen stream because of the size of the microchip. A Karman vortex formed on the opposite side of the microfluidic chip. For this reason, the cold nitrogen stream was distributed and this decreased the cooling rate. Thus, flash cooling was not achieved using a standard microfluidic chip. Therefore, we did not obtain a clear X-ray diffraction pattern using a standard microfluidic chip under the cryogenic condition tested. However, the microfluidic chip that was cut to the size of 5 × 5 mm^2 was placed completely in the nitrogen stream and frost was not observed (Figure 3b). These results suggest the size of the microfluidic chip is a significant factor for in situ X-ray diffraction experiments.

In the case of a batchwise procedure, cryoprotection involving the soaking of a protein crystal in a highly concentrated cryoprotectant solution has been shown to deteriorate the protein crystal because of osmotic shock.[34] In some cases, there is the possibility of cracking the protein crystal. However, our microfluidics-based approach avoids damage to the crystal during cryoprotection as mentioned above. To confirm the effect of the stepwise cryoprotection, the mixing time per one manipulation was changed to 5, 10, and 30 min. For the microfluidics-based approach, deterioration of the lysozyme crystal was not observed in any mixing period under the optical microscopic measurement. Figure 4 shows

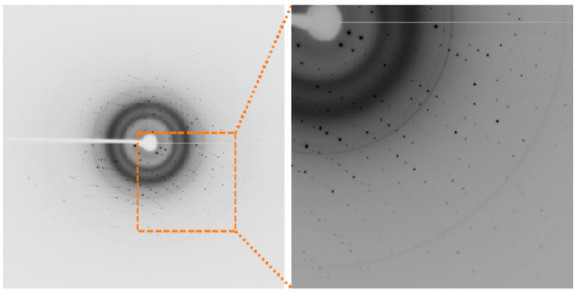

Figure 4. Diffraction image of a lysozyme crystal from the on-chip X-ray diffraction experiment at 100 K. The lysozyme crystal diffracted to a resolution limit of 1.6 Å.

diffraction images of a lysozyme crystal from an on-chip X-ray diffraction experiment at 100 K. As shown in Figure 4, the ice ring was not observed, and the diffraction pattern at the high-angle (high resolution) was confirmed with low background. The diffraction data was analyzed by XDS software and CCP4 suite of programs. Table 1 shows the results of the crystallographic data. Measurement temperature of lysozyme crystals without cryoprotection and cryocooled lysozyme crystals were 277 and 100 K, respectively. The lysozyme crystal without cryoprotection diffracted to a resolution limit of 1.8 Å. In contrast, the cryocooled lysozyme crystals diffracted to a resolution limit of 1.6 Å regardless of the mixing time. The space groups of the lysozyme crystals were not different between the samples prepared with or without cryoprotection. However, cell dimensions were slightly different. The lattice constant of the cryocooled lysozyme crystals is smaller than the nontreated lysozyme crystal. We previously reported this phenomenon by using droplet-based protein crystallization.[24] Protein crystals contain many water molecules in the crystal lattice. Hence, the lattice constant of a protein crystal decreases because of rapid dehydration that occurs with cryoprotection. In addition, this rapid dehydration induces the increase of mosaicity. Generally, the mosaicity of a lysozyme crystal with traditional cryoprotection is ∼0.3.[16,35] However, mosaicity and completeness were identical, as shown in Table 1, regardless of cryoprotection, although the value of completeness of the outer shell without cryoprotection was found to decrease gradually. We consider that the stepwise cryoprotection makes it possible to obtain the low mosaicity crystallographic data. Conversely, the nontreated lysozyme crystal was damaged by X-ray radiation.

Figure 5a shows the relationship between resolution range and I/σ (I). In brief, I/σ (I) represents the S/N ratio. Typically,

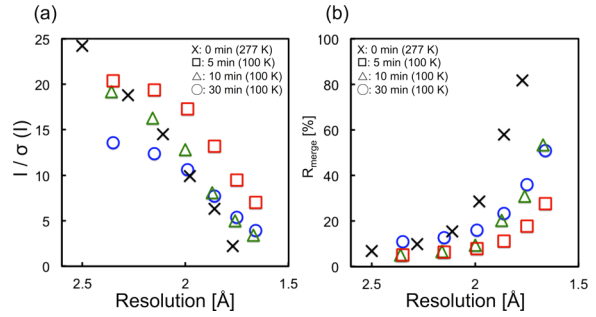

Figure 5. (a) Relationship between resolution range and I/σ (I). (b) Relationship between resolution range and R_{merge}. Measurement temperature was 100 and 277 K for the cryocooled lysozyme crystals and the lysozyme crystal without cryoprotection, respectively.

the data of I/σ (I) of the outer shell are more than 2 for crystal structure analysis. When X-ray irradiation damages the lysozyme crystal, the value of I/σ (I) in the high-resolution range is reduced. The value of I/σ (I) of the lysozyme crystal without cryoprotection was found to linearly decrease when compared with the cryoprotected lysozyme crystals, as shown

Table 1. Results of Crystallographic Data of Lysozyme Crystals[a]

	0 min (277 K)[b]	30 min (100 K)[c]	10 min (100 K)[c]	5 min (100 K)[c]
space group	$P4_32_12$	$P4_32_12$	$P4_32_12$	$P4_32_12$
dimensions (Å)	$a = b = 79.31$ $c = 37.86$	$a = b = 78.96$ $c = 37.03$	$a = b = 78.88$ $c = 37.06$	$a = b = 78.61$ $c = 37.03$
resolution (Å)	39.65−1.77 (1.86−1.77)	39.48−1.66 (1.75−1.66)	39.06−1.67 (1.76−1.67)	39.30−1.66 (1.75−1.66)
mosaicity (deg)	0.11	0.17	0.26	0.17
completeness (%)	93.1 (85.9)	99.2 (96.7)	96.6 (98.4)	97.9 (99.0)
R_{merge} (%)	6.2 (81.8)	13.0 (51.0)	6.5 (53.4)	6.4 (27.6)
I/σ (I)	21.1 (3.2)	10.5 (3.9)	15.6 (3.4)	17.5 (7.0)

[a]Values inside the parentheses represents the data of the outer shell. [b]Data of the lysozyme crystal without cryoprotection at 277 K. [c]Data of the cryocooled lysozyme crystal with different mixing times.

DOI: 10.1021/acs.analchem.5b00151
Anal. Chem. 2015, 87, 4194−4200

in Figure 5 a. Generation of oxygen radicals is believed to be the cause of radiation damage. The lysozyme crystals were rarely generated in the same crystallization chamber. We analyzed these crystals by X-ray diffraction measurements at 277 K and found the radiation damage did not propagate to another crystal generated in the same crystallization chamber because of the short lifetime of the oxygen radical (data not shown). In contrast, the value of I/σ (I) of the lysozyme crystals that underwent cryoprotection was found to gradually decrease even in the high-resolution range. However, the decreasing rates of I/σ (I) of cryoprotected lysozyme crystals were found to be slightly smaller than the nontreated lysozyme crystal, especially at the high-resolution range. The change of I/σ (I) in the resolution range between 2 and 1.6 Å strongly suggests that the nontreated lysozyme crystal was damaged more by the X-ray radiation than the cryoprotected lysozyme crystal. In comparison between mixing times of the cryoprotectant solution, the lysozyme crystal showed stepwise cryoprotection up to 5 min with the highest quality diffraction data. Figure 5b shows a relationship between resolution range and R_{merge}. R_{merge} is a reliability factor in the field of crystallography. Generally, the data of R_{merge} of the outer shell should be <30% for crystal structure analysis. The value of R_{merge} of the nontreated lysozyme crystal has the highest value in all resolution ranges. Conversely, the lysozyme crystal with 5 min cryoprotection was a diffraction-quality crystal even in that high-resolution range. These results suggest stepwise cryoprotection via the microfluidic chip and in situ X-ray analysis is an effective method for protein crystal structure analysis.

To characterize the effect of cryoprotection, we analyzed the value of I/σ (I) of lysozyme crystals under each cryoprotection condition in steps of 10 images. Figure 6 shows a relationship

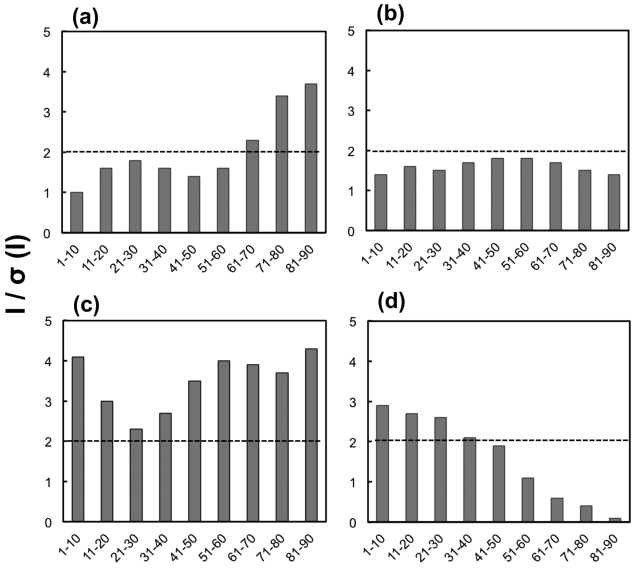

Figure 6. Relationship between I/σ (I) of the outer shell and the diffraction images. The mixing time per one manipulation was (a) 30 min, (b) 10 min, (c) 5 min, and (d) 0 min (without cryoprotection).

between I/σ (I) of the outer shell and the diffraction images. As a result, the value of I/σ (I) was influenced significantly by the cryoprotection and the mixing time. Reduction of I/σ (I) with increasing irradiation time was not observed, as shown in Figure 6a–c. In other words, cryocooled lysozyme crystals did not undergo radiation damage. However, lysozyme crystals without cryoprotection showed a reduction of I/σ (I) with increasing irradiation time (Figure 6d). In particular, the value of I/σ (I) decreased to less than 2 from 41 to 90 images. The X-ray measurement was carried out with an exposure time of 30 s, and the oscillation angle was 1°. This result suggests that the lysozyme crystal was degraded by synchrotron radiation of 20 min. The lysozyme crystal that underwent stepwise cryoprotection over 5 min showed the highest quality crystallographic data. The value of I/σ (I) was more than 2 during the X-ray measurement. However, the lysozyme crystal subjected to cryoprotection over 30 min intervals showed lower quality when compared with the other cryoprotected lysozyme crystals. We consider that stepwise cryoprotection was able to prevent osmotic shock caused by the rapid increase of the cryoprotectant concentration. Conversely, the lysozyme crystal subjected to cryoprotection at a set period was slightly damaged by osmotic shock. Consequently, the value of I/σ (I) was less than 2 at oscillation angles of 1–60° (Figure 6a). Figure 7

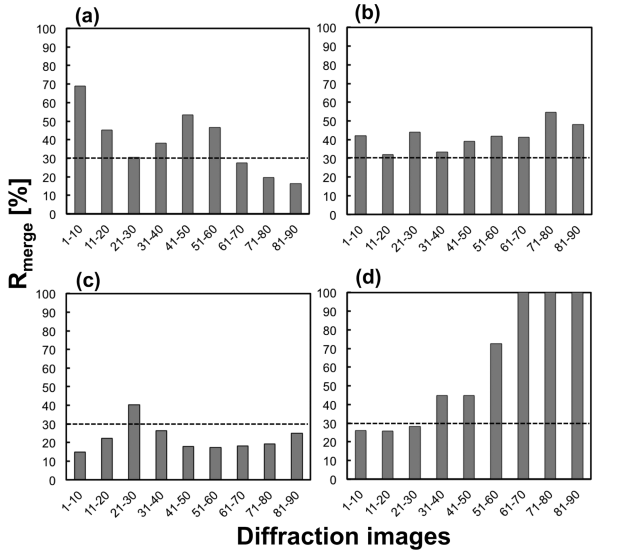

Figure 7. Relationship between R_{merge} of the outer shell and the diffraction images. The mixing time per one manipulation was (a) 30 min, (b) 10 min, (c) 5 min, and (d) 0 min (without cryoprotection).

shows a relationship between R_{merge} of the outer shell and diffraction images. We also examined the R_{merge} of lysozyme crystals of each cryoprotection condition in steps of 10 images. The mixing time of the cryoprotectant solution also affected the R_{merge} value, and the lysozyme crystal treated by stepwise cryoprotection for 5 min showed the best result compared with the other conditions (Figure 7 c). Additionally, when we employed short-step cryoprotection, a variation of the R_{merge} value was scarcely observed. For lysozyme crystals without cryoprotection, the value of R_{merge} was found to increase rapidly with increasing exposure time. In particular, the value of R_{merge} from 51 to 90 was dramatically increased (Figure 7 d). Therefore, the average value of R_{merge} of the outer shell was calculated to be 81.8%, as shown in Table 1. However, the crystallographic data from 1 to 30 were sufficient for analyzing the crystal structure determination, e.g., the lysozyme crystal without cryoprotection measured at 277 K maintained diffraction quality over a short period. The degree of deterioration depends on the measurement conditions. When we employed the high-flux X-ray beamline, the protein crystal was immediately damaged by radiation, especially the non-

DOI: 10.1021/acs.analchem.5b00151
Anal. Chem. 2015, 87, 4194–4200

treated protein crystal. However, the cryoprotection procedure required very careful handling of the protein crystal. Thus, the combination of the microfluidic chip developed in this study and the high-flux beamline offers high-throughput measurements. The microfluidic chip for cryoprotection integrated six crystallization chambers within one device. Cryoprotection can be conducted simultaneously at the all crystallization chambers without any complicated handling of protein crystal. The high-throughput capability can be increased by increasing the number of crystallization chambers within a microfluidic chip. The final size of the microfluidic chip was 5×5 mm^2, as shown in Figure 3b. Although the time necessary to collect diffraction data set strongly depends on the performance of beamline, our microfluidic-based method can eliminate additional procedures and time for pretreatment of X-ray analysis. In addition, our method is able to avoid the damage from manual handling of protein crystal on the cryoprotection procedure. Therefore, microfluidics-based cryoprotection introduced in this study can be used for high-throughput crystal structure analysis of protein microcrystals using a high-flux synchrotron X-ray beam.

CONCLUSIONS

We have introduced a contactless cryoprotection method that avoids damage to the sample using a microfluidic chip for X-ray protein crystal structure analysis. We can also conduct a seamless procedure from protein crystallization to X-ray analysis. Hence, the microfluidic-based approach reported in this paper is a user-friendly interface for novices of X-ray analysis of protein crystals. We determined a suitable size of the microfluidic chip for in situ X-ray analysis under cryogenic conditions. The quality of the lysozyme crystal without cryoprotection was found to decrease gradually with increasing measurement time. In contrast, the lysozyme crystal with cryoprotection did not show any deterioration of the crystallographic quality. We also investigated the effect of stepwise cryoprotection on the quality of the lysozyme crystal. The mixing time of the cryoprotectant affected the quality of the lysozyme crystal. The short-step cryoprotection method prevented osmotic shock caused by soaking the crystal in the cryoprotectant, and the crystals produce high-quality diffraction crystallographic data. Consequently, we can obtain a complete diffraction data set of lysozyme crystals to determine the 3D structure without any complicated manipulations. We believe that the microfluidics-based method demonstrated above can facilitate protein structure determination, including membrane proteins, with high resolution. Obtaining a large membrane protein single crystal that is >100 μm is one of the most difficult issues in protein structure determination. Therefore, our method provides a solution for researchers who conduct protein crystallography and structural biology. In this study, we showed the possibility of a microfluidic-based approach that the end user can use for protein 3D structure determination.

AUTHOR INFORMATION

Corresponding Authors

*E-mail: m.maeki@eng.hokudai.ac.jp. Tel.: +81-11-706-6745. Fax: +81-11-706-6745.

*E-mail: m.miyazaki@aist.go.jp. Tel.: +81-942-81-4059. Fax: +81-942-81-3627.

Notes

The authors declare no competing financial interest.

ACKNOWLEDGMENTS

A part of this work was supported by a Grant-in-Aid for JSPS Fellows 26·7016 (to M. Maeki). This work was also carried out under the Cooperative Research Program "Network Joint Research Center for Materials and Devices". We thank beamline staff of BL9 at SAGA Light Source for data collection. A part of the X-ray diffraction experiments were carried out at the Kyushu Synchrotron Light Research Center Beamline (SAGA-LS/BL07) with proposal no. 1305053P.

REFERENCES

(1) Sun, H.; Scott, D. O. *Chem. Biol. Drug Des.* **2010**, *75*, 3−17.
(2) Congreve, M.; Marshall, F. *Br. J. Pharmacol.* **2010**, *159*, 986−996.
(3) Drinkwater, N.; McGowan, S. *Biochem. J.* **2014**, *461*, 349−369.
(4) Schmidt, T.; Bergner, A.; Schwede, T. *Drug Discovery Today* **2014**, *19*, 890−897.
(5) Chayen, N. E. *Curr. Opin. Struct. Biol.* **2004**, *14*, 577−583.
(6) Krauss, I. R.; Merlino, A.; Vergara, A.; Sica, F. *Int. J. Mol. Sci.* **2013**, *14*, 11643−11691.
(7) Weierstall, U.; James, D.; Wang, C.; White, T. A.; Wang, D.; Liu, W.; Spence, J. C. H.; Doak, R. B.; Nelson, G.; Fromme, P.; Fromme, R.; Grotjohann, I.; Kupitz, C.; Zatsepin, N. A.; Liu, H.; Basu, S.; Wacker, D.; Han, G. W.; Katritch, V.; Boutet, S.; Messerschmidt, M.; Williams, G. J.; Koglin, J. E.; Seibert, M. M.; Klinker, M.; Gati, C.; Shoeman, R. L.; Barty, A.; Chapman, H. N.; Kirian, R. A.; Beyerlein, K. R.; Stevens, R. C.; Li, D.; Shah, S. T. A.; Howe, N.; Caffrey, M.; Cherezov, V. *Nat. Commun.* **2014**, *5*, 3309−3314.
(8) Baba, S.; Hoshino, T.; Ito, L.; Kumasaka, T. *Acta Crystallogr., Sect. D* **2013**, *69*, 1839−1849.
(9) Sugahara, M. *PLoS One* **2014**, *9*, e95017.
(10) Thorne, R. E.; Stum, Z.; Kmetko, J.; O'Neill, K.; Gillian, R. *J. Appl. Crystallogr.* **2003**, *36*, 1455−1460.
(11) Petsko, G. A. *J. Mol. Biol.* **1975**, *96*, 381−392.
(12) Garman, E. *Curr. Opin. Struct. Biol.* **2003**, *13*, 545−551.
(13) Li, L.; Ismagilov, R. F. *Annu. Rev. Biophys.* **2010**, *39*, 139−158.
(14) Hansen, C. L.; Skordalakes, E.; Berger, J. M.; Quake, S. R. *Proc. Natl. Acad. U.S.A.* **2002**, *99*, 16531−16536.
(15) Shim, J.; Cristobal, G.; Link, D. R.; Thorsen, T.; Jia, Y.; Piattelli, K.; Fraden, S. *J. Am. Chem. Soc.* **2007**, *129*, 8825−8835.
(16) Guha, S.; Perry, S. L.; Pawate, A. S.; Kenis, P. J. A. *Sens. Actuators, B* **2012**, *174*, 1−9.
(17) Maeki, M.; Teshima, Y.; Yoshizuka, S.; Yamaguchi, H.; Yamashita, K.; Miyazaki, M. *Chem.—Eur. J.* **2014**, *20*, 1049−1056.
(18) Ildefonso, M.; Candoni, N.; Veesler, S. *Cryst. Growth Des.* **2011**, *11*, 1527−1530.
(19) Hirata, K.; Itoh, K. S.; Yano, N.; Takemura, S.; Kato, K.; Hatanaka, M.; Muramoto, K.; Kawahara, T.; Tsukahara, T.; Yamashita, E.; Tono, K.; Ueno, G.; Hikima, T.; Murakami, H.; Inubushi, Y.; Yabashi, M.; Ishikawa, T.; Yamamoto, M.; Ogura, T.; Sugimoto, H.; Shen, J. R.; Yoshikawa, S.; Ago, H. *Nat. Methods* **2014**, *11*, 734−736.
(20) Smith, J. L.; Fischetti, R. F.; Yamamoto, M. *Curr. Opin. Struct. Biol.* **2012**, *22*, 602−612.
(21) Zheng, B.; Tice, J. D.; Roach, L. S.; Ismagilov, R. F. *Angew. Chem., Int. Ed.* **2004**, *43*, 2508−2511.
(22) Hansen, C.; Classen, S.; Berger, J. M.; Quake, S. R. *J. Am. Chem. Soc.* **2006**, *128*, 3142−3143.
(23) Perry, S. L.; Guha, S.; Pawate, A. S.; Bhaskarla, A.; Agarwal, V.; Nair, S. K.; Kenis, P. J. A. *Lab Chip* **2013**, *13*, 3183−3187.
(24) Maeki, M.; Yoshizuka, S.; Yamaguchi, H.; Kawamoto, M.; Yamashita, K.; Nakamura, H.; Miyazaki, M.; Maeda, H. *Anal. Sci.* **2012**, *28*, 65−68.
(25) Liu, Y.; Wang, X.; Ching, C. B. *Cryst. Growth Des.* **2010**, *10*, 548−558.
(26) Unger, M. A.; Chou, H. P.; Thorsen, T.; Scherer, A.; Quake, S. R. *Science* **2000**, *288*, 113−116.
(27) Thorsen, T.; Maerkl, S. J.; Quake, S. R. *Science* **2002**, *298*, 580−584.

DOI: 10.1021/acs.analchem.5b00151
Anal. Chem. 2015, 87, 4194−4200

(28) Mohan, R.; Schudel, B. R.; Desai, A. V.; Yearsley, J. D.; Apblett, C. A.; Kenis, P. J. A. *Sens. Actuators, B* **2011**, *160*, 1216−1223.
(29) Lopez-Jaramillo, F. J.; Garcia-Ruiz, J. M.; Gavira, J. A.; Otalora, F. *J. Appl. Crystallogr.* **2001**, *34*, 365−370.
(30) Kabsch, W. *Acta Crystallogr., Sect. D* **2010**, *66*, 125−132.
(31) Collaborative Computational Project, Number 4*Acta Crystallogr., Sect. D*, **1994**, *50*, 760−763.
(32) Garman, E. F.; Schneider, T. R. *J. Appl. Crystallogr.* **1997**, *30*, 211−237.
(33) Bujacz, G.; Wrzesniewska, B.; Bujacz, A. *Acta Crystallogr., Sect. D* **2010**, *66*, 789−796.
(34) Jaramillo, F. J. L.; Moraleda, A. B.; Ramirez, L. A. G.; Carazo, A.; Ruiz, J. M. G. *Acta Crystallogr., Sect. D* **2002**, *58*, 209−214.
(35) Sugahara, M. *J. Appl. Crystallogr.* **2012**, *45*, 362−366.

DOI: 10.1021/acs.analchem.5b00151
Anal. Chem. 2015, 87, 4194−4200